

Using Seismic Attributes in seismotectonic research: an application to the Norcia's Mw=6.5 earthquake (30th October 2016) in Central Italy.

Maurizio Ercoli^{1*}, Emanuele Forte², Massimiliano Porreca^{1*}, Ramon Carbonell³, Cristina Pauselli^{1*}, Giorgio Minelli^{1*}, Massimiliano R. Barchi^{1*}.

¹ Dip. di Fisica e Geologia – Università degli Studi di Perugia (Perugia, Italy).

² Dept. of Mathematics and Geosciences, University of Trieste (Trieste, Italy).

³ Dept. Structure & Dynamics of the Earth, CSIC-Inst. Earth Sciences Jaume Almera (Barcelona, Spain).

*member of Interuniversity Center for Research on 3D-Seismotectonics (Centro InterUniversitario per l'Analisi SismoTettonica tridimensionale con applicazioni territoriali – CRUST).

Correspondence to: Maurizio Ercoli (maurizio.ercoli@unipg.it; maurizio.ercoli@gmail.com)

Abstract. In seismotectonic studies, seismic reflection data are a powerful tool to unravel the complex deep architecture of active faults. Such tectonic structures are usually mapped at surface through traditional geological surveying whilst seismic reflection data may help to trace their continuation from the near-surface down to hypocentral depth. In this study, we propose the application of the seismic attributes technique, commonly used in seismic reflection exploration by oil industry, to seismotectonic research for the first time. The study area is a geologically complex region of Central Italy, recently struck by a long-lasting seismic sequence including a Mw 6.5 main-shock. A seismic reflection data-set consisting of three vintage seismic profiles, currently the only available across the epicentral zone, constitutes a singular opportunity to attempt a seismic attribute analysis. ~~This analysis resulted in peculiar seismic signatures which generally correlate with the exposed surface geologic features, and also confirming the presence of other debated structures.~~ These results are critical, because provide information also on the relatively deep structural setting, mapping a prominent, high amplitude regional reflector ~~that marks~~ the top basement, interpreted as important rheological boundary. Complex patterns of high-angle discontinuities crossing the reflectors have ~~been also~~ identified. These dipping fabrics are interpreted as the expression of fault zones, belonging to the active normal fault systems responsible for the seismicity of the region. This work demonstrates that seismic attribute analysis, even if used on low-quality vintage 2D data, may contribute to improve the subsurface geological interpretation of areas characterized by high seismic potential.

1 Introduction



Studying the connections between the earthquakes and the faults to which they are associated is a primary assignment of seismotectonics (Allen et al., 1965; Schwartz and Coppersmith, 1984). Clearly, this is not an easy task: it is in fact generally complex to fill the gap between the exposed geology including the active “geological faults” mapped by the geologists and

31 the seismic features describing the geometry and kinematics of the seismic source at hypocentral depth (“seismological
32 faults”, e.g. Barchi & Mirabella, 2008).

33 In case of strong earthquakes, impressive topographic changes and surface ruptures are often reported (e.g. Press and
34 Jackson, 1965; Wyss & Brune, 1967; Jibson et al., 2018; Yi et al., 2018; Civico et al, 2018). While many studies on the
35 surface geology are generally performed, especially after important events, the recovery of deep information on the
36 seismogenic structures is always a challenge, primarily due to the lack of high-resolution geophysical data and/or wells
37 stratigraphy.

38 This fact generates uncertainties that may amplify the scientific debate and the number of models introduced by the
39 geoscientists. Therefore, this process requires the use of appropriate geophysical data, aimed at recovering information on
40 the deep geological architecture and, in particular, on the geometry of active faults.

41 Different geophysical methods (e.g. Gravimetry, Magnetics, Electric and Magnetotellurics, Ground Penetrating Radar) may
42 contribute to define the stratigraphy and structural setting of the upper crust at different scales. But the seismic reflection is
43 largely the most powerful tool producing high-resolution images fundamental to trace the actual geometry of active faults at
44 surface (usually mapped and reconstructed in geological cross-sections), from the near surface down to hypocentral depths.
45 However, the ex-novo acquisition of onshore deep reflection data, possibly 3D, is often hampered by environmental
46 problems, complex logistics, and high costs. These issues seriously limit the possible widespread use of this technique for
47 scientific research. Significant exceptions are research projects for deep crustal investigations like BIRPS (Brewer et al.,
48 1983), CoCORP (Cook et al., 1979), ECORS (Roure et al., 1989) and CROP (Barchi et al., 1998; Finetti et al., 2001),
49 IBERSEIS (Simancas et al., 2003).

50 Such limitations can be partially overcome by considering old profiles (legacy data) acquired by the exploration industry.
51 When collected in seismically active regions, such data may be used to connect the active faults mapped at the surface with
52 the seismogenic sources depicted by seismological recordings (Boncio et al., 2000; Bonini et al., 2014; Carvalho et al., 2008;
53 Beidinger et al., 2011; Maesano et al., 2015; Porreca et al., 2018). Vintage profiles can therefore significantly contribute to
54 seismotectonic research, even if their location and orientation were not specifically designed with this aim. In addition,
55 seismic technologies and acquisition/processing strategies of some decades ago, produced data with both relatively low
56 signal/noise ratio (S/N) and resolution in comparison to modern data.

57 To improve the data quality and increase the accuracy of the interpretation, three main strategies can be usually considered:
58 1) collection of new reflection seismic data with modern technologies, optimizing feasibility studies on the base of available
59 vintage datasets; 2) reprocessing of the old data from raw to new stacks using new and available powerful capabilities and
60 developments and, 3) use post-stack processing techniques such as seismic attributes analysis. These approaches are
61 currently all used by the O&G industry (e.g. in the re-assessment of known reservoirs) and are clearly characterized by
62 different potential, costs and working time.

63 Some limitations characterize the first two approaches: the first is particularly demanding in terms of costs and logistic, and
64 not practicable in zones where the use of dynamite or arrays of vibroseis trucks is forbidden or limited (e.g. National Parks

65 or urban areas). The second requires broad projects encompassing specialized teams, high-computation power and generally
66 long processing times, the latter is dependent on the quality of the raw data. The third strategy, in the case of the attribute
67 analysis exploits a well-known and mature technique. It has been used since early 80's by the O&G exploration industry
68 (Chopra & Marfurt, 2005) for geometrical and petrophysical characterization of reservoirs (Chopra & Marfurt, 2008).
69 A seismic attribute is a quantity derived from seismic data (pre-stack and/or post-stack) that can be calculated on a single
70 trace, on multiple traces, or volumes. This technique is commonly used to extract additional information that may be unclear
71 in a traditional seismic image, therefore leading to a better interpretation of the data. Examples of applications on dense 3D
72 seismic volumes produced spectacular results (Chopra & Marfurt, 2007; Marfurt et al., 2011; Hale, 2013; Barnes, 2016,
73 Marfurt, 2018). Recent developments of approaches based on machine learning techniques are currently pushing it further to
74 contribute towards an objective (automatic) interpretation of seismic data-sets (Wrona et al., 2018; Di & AlRegib, 2019;
75 Naeini & Prindle, 2019). Therefore, among the three strategies, the attribute analysis is probably the easiest, cheapest and
76 fastest to qualitatively emphasize the geophysical features and data properties of reflection seismic data sets in complex
77 geological areas. Due to different well-known limitations and advantages existing between 2D vs 3D seismic data (these are
78 extensively discussed by Torvela et al. (2013) and Hutchinson (2016), 2D seismic attribute analysis of post-stack data may
79 be subjected to possible pitfalls and/or may not bring so impressive improvements in the seismic images. However, the main
80 point is that inland, most of the sedimentary basins have actually been sampled by 2D grids of seismic profiles, or at least
81 they have been probed by a few sparse 2D seismic lines. Hence, it is relevant to extract as much information as possible from
82 these 2D surveys in areas not covered by 3D seismic surveys. Whilst in the hydrocarbon industry this process is useful even
83 if mainly driven by a constant necessity to reduce the costs (Ha et al., 2019), in seismotectonic researches it is affected by
84 even worse limitations previously aforementioned. Therefore, also slight improvements obtained on vintage 2D data may
85 bring to new and unprecedented subsurface information in complex and active tectonic environments. We think that we might
86 successfully export a similar approach in a seismotectonic study applying this type of analysis on an active seismic zone,
87 covered only by a very limited number of 2D seismic lines. Based on such considerations, the selected study area is located
88 in the central Apennines (Central Italy), a region between the southeastern part of the Umbria-Marche Apennines and the
89 Laga Domain in the outer Northern Apennines (e.g. Barchi et al., 2001). This area presents ideal characteristics to test the
90 proposed new approach. In fact, in the past, several seismic profiles were acquired at this location for hydrocarbon
91 exploration, providing good constraints for subsurface geological interpretation (Bally et al., 1986; Barchi et al, 1991; Barchi
92 et al., 1998; Ciaccio et al., 2005; Pauselli et al., 2006; Mirabella et al. 2008; Barchi et al., 2009; Bigi et al., 2011). After the
93 last 2016-2017 seismic sequence, Porreca et al. (2018) have provided a new regional geological model based on the
94 interpretation of vintage 2D seismic lines. In such a study, the authors remark important differences in the seismic data
95 quality across the region. In fact, the eastern area that shows higher overall data quality, is located at the footwall of the
96 Mount Sibillini thrust (MSt) and, includes (consists of) flyschoid units of the Laga foredeep Domain. It is noteworthy that
97 the Mw 6.5 epicentral zone, is located on the MSt hanging-wall (Lavecchia, 1985). This is characterized by prevalent
98 carbonate sequence and, its crossed by seismic sections with lower S/N ratio, that hampered the subsurface interpretation.

99 Therefore, this contribution focuses on three low quality seismic cross-sections located close to the Mw 6.5 main-shock area,
100 aiming to exploit the use of seismic attributes to squeeze additional information. The main goal of this study is to obtain as
101 much information as possible on the geological structures responsible for the seismicity. Therefore, any improvement, that
102 for example can increase the resolution, the definition and/or the lateral continuity of the structural features is a very valuable
103 contribution. The current manuscript is an example of how can seismic attribute analysis contribute to seismotectonic
104 research as an innovative approach.

105 2 Geological framework and seismotectonics of the study area

106 During the 2016-2017, a wide part of Central Italy has been struck by a complex seismic sequence, characterized by multi-
107 fault ruptures occurred within few months (August 2016 – January 2017) similarly to previous seismic sequences in Central
108 Italy (e.g. L'Aquila and Colfiorito, Valoroso et al., 2013 and Chiaraluce et al., 2005). ~~Nine earthquakes with M>5 and more
109 that 97'000 events in two years have been recorded at hypocentral depth not exceeding 12 km (Fig.1).~~ The strongest
110 mainshock of Mw 6.5 occurred on 30th October 2016 (Chiaraluce et al., 2017; Chiarabba et al., 2018; Gruppo di Lavoro
111 Sequenza Centro Italia, 2019; Improta et al., 2019; ISIDe working group, 2019), generating impressive co-seismic ruptures
112 (Civico et al., 2018; Brozzetti et al., 2019).

113 The study area is located in the easternmost part of the Northern Apennines fold and thrust belt, including the Umbria-
114 Marche thrust and fold belt domain and Laga Formation. This is a geologically complex region, where in the past the
115 analysis of 2D seismic profiles have produced contrasting interpretation of the upper crust structural setting, e.g. thin vs.
116 thick skinned tectonics, fault reactivation/inversion, basement depth (Bally et al., 1986; Barchi, 1991; Barchi et al., 2001;
117 Bigi et al., 2011; Calamita et al., 2012; Porreca et al., 2018). The Umbria-Marche fold and thrust belt was formed during the
118 Miocene compressive phase, and overthrusts the Laga foredeep sequence, through arc-shaped major thrusts, namely the M.
119 Sibillini thrust (MSt, Koopman, 1983; Lavecchia, 1985), with eastward convexity. The compressional structures were later
120 disrupted by the extensional faults since the Late Pliocene.

121 The Umbria-Marche domain involves the rocks of the sedimentary cover, represented by three main units:

- 122 1) ~~on top,~~ the Laga sequence consisting of siliciclastic turbidites belonging to the Laga foredeep and foreland Formation
123 (Milli et al., 2007; Bigi et al., 2011); it is made by alternating layers of sandstones, marls and evaporites (Late Messinian –
124 Lower Pliocene, up to 3000 m thick, average seismic velocity (v_{av})= 4000 m/s), mainly outcropping in the eastern sector of
125 the study area (i.e. at the footwall of the MSt). 
- 126 2) ~~in the middle,~~ carbonate formations (Jurassic-Oligocene, about 2000 m thick, v_{av} = 5800 m/s) formed by pelagic
127 limestones (Mirabella et al., 2008) with subordinated marly levels overlying an early Jurassic carbonate platform (Calcare
128 Massiccio Fm.)
- 129 3) ~~at the bottom,~~ Late Triassic evaporites (1500–2500 m thick, v_{av} = 6400 m/s), consisting in alternated layers of anhydrites
130 and dolomites (Anidriti di Burano Fm. And and Raethavicula Contorta beds; Martinis & Pieri, 1964), never outcropping and

131 intercepted, only, by deep wells (Porreca et al., 2018 and references therein), representing the main and deeper detachment of
132 the region.

133 An underlying basement of variable lithology ($v_{av} = 5100$ m/s) that never crops out (Vai, 2001), was intercepted by deep
134 wells (Bally et al., 1986; Minelli & Menichetti, 1990; Anelli et al., 1994; Patacca & Scandone, 2001) and, it is separated by
135 the aforementioned units by the aforementioned important regional decollement.

136 In a such complex structural setting, the Late Pliocene-Quaternary extensional tectonic phase, characterized by a prevalent
137 NE-SW stretching direction, produced NNW-SSE striking WSW-dipping normal faults. These faults were also responsible of
138 the tectono-sedimentary evolution of intra-mountain continental basins (Calamita et al., 1994; Cavinato and De Celles, 1999).
139 The most evident Quaternary basins of this part of the Apennines are the Castelluccio di Norcia (CNb) and Norcia (Nb) basins,
140 located respectively at 1270 and 700 m a.s.l. They have been subjected to a lacustrine and fluvial sedimentation of hundreds
141 of meters characterized by fine clayey to coarse grained deposits (Blumetti et al., 1993; Coltorti and Farabollini, 1995).

142 The area is affected by historical and instrumental seismicity with frequent small to moderate magnitude earthquakes ($4 <$
143 $M_w < 7$, Boncio and Lavecchia, 2000; Rovida et al., 2016). The recent 2016-2017 seismic sequence has been caused by the
144 activation of a complex NNW-SSE trending fault system, characterized by prevalent high-angle WSW-dipping normal faults
145 (Lavecchia et al., 2016). More in detail, the easternmost fault system of the region recently activated is the NNW-SSE
146 trending "Monte Vettore fault system" (Vf). This was the responsible of the mainshock nucleation between the continental
147 Norcia (Nb) and Castelluccio di Norcia basins (CNb) (Fig. 1). Nb and CNb are two asymmetrical grabens, bordered by high-
148 angle WSW-dipping normal faults located on their eastern flanks. Both fault systems are thought to have high seismogenic
149 potential and able to generate earthquakes up to $M_w 7.0$ (e.g. Barchi et al., 2000; Basili et al., 2008; Rovida et al., 2016;
150 DISS Working Group, 2018).

151 The Nb master fault (Nottoria-Preci fault, Nf) is considered responsible of the 1979 earthquake (Deschamps et al., 1984;
152 Brozzetti & Lavecchia, 1994; Rovida et al., 2016) and possibly associated to multiple historical events (Galli et al., 2005;
153 Pauselli et al., 2010; Galli et al., 2018), including the 1703 ($M_e = 6.8$, Rovida et al., 2016). The CNb master fault (Vf) and its
154 secondary splays activated during the 2016-2017 sequence (e.g. Wilkinson et al., 2017; Villani et al., 2018a) were already
155 known and mapped due to paleo-seismological and shallow geophysical evidences (Galadini & Galli, 2003; Galli et al.,
156 2008; Ercoli et al., 2013; Ercoli et al., 2014). However, despite of the large amount of surface data collected (Livio et al.,
157 2016; Pucci et al., 2017; Wilkinson et al., 2017; De Guidi et al., 2017; Brozzetti et al., 2019; Galli et al., 2018), the deep
158 extension of the Norcia and Castelluccio faults (particularly the Vf), and the overall complex structure of the area are still
159 debated (Lavecchia et al., 2016; Porreca et al., 2018; Bonini et al., 2019; Cheloni et al., 2019; Improta et al. 2019).

160 **3 Data**

161 We have performed the seismic attributes analysis on three W-E trending 2D seismic reflection profiles crossing the
162 epicentral area between the Umbria and Marche regions (Central Italy, Fig.1). Such 2D data are part of a much larger,

163 unpublished dataset including 97 seismic profiles and few boreholes, drilled for hydrocarbon exploration by ENI in the
164 period 1970-1998.

165 The data quality is extremely variable (medium/poor) with limited fold (generally < 60 traces / Common Mid-Point - CMP)
166 mainly due to environmental and logistical factors like: acquisition technologies, limited site access, complex tectonic
167 setting, and different (contrasting) outcropping lithologies like Carbonates and Quaternary sediments that resulted often in
168 low S/N recordings (e.g. Mazzotti et al., 2000, Mirabella et al., 2008).

169 The analysed lines include: NOR01 (stack, 14 km long), NOR02 (time-migrated, 20 km long, partially parallel to NOR01 on
170 the western sector), and CAS01 (stack, 16 km long), located more to the south (Fig. 1). NOR01 and CAS01 were acquired
171 using a Vibroseis source, whilst explosive was used for NOR02; all the lines are displayed in Two-Way-Travel-Time
172 (TWTT) limited to 4.5 s. The average frequency spectra display bandwidths ranging from few Hz up to 60-70 Hz, whilst
173 NOR02 extends up to 100 Hz. Assuming the average peak frequency of 20 Hz, a vertical resolution of ca. 80 m can be
174 estimated (average carbonate velocity = 6 km/s, parameters in Table 1s, supporting information). Some processing artefacts
175 (A) are visible in NOR01 as a straight horizontal signal at ca. 1 s (Fig. 2a), and two others sub-horizontal between 1-2 s in
176 CAS01 (Fig. 1s-a, supporting information). However, some seismic events and lineaments, related to geological structures of
177 interest, are slightly visible and their display seems potentially improvable with a proper choice of seismic attributes type
178 and parameters. Therefore, we loaded the lines into the **OpenTect (OdT) software**, setting up a common seismic datum
179 equal to 500 m while adding some ancillary data, extracted by a complementary GIS (**QGis software**) project including:
180 regional fault patterns (**from maps and Ithaca database**), a regional DTM (Tarquini et al., 2007; Tarquini et al., 2012),
181 geological maps (Pierantoni et al., 2013; Carta Geologica Regionale 1:10'000 – Regione Marche, 2014; Carta Geologica
182 Regionale 1:10'000 – Regione Umbria, 2016), as well as mainshock earthquakes distribution belonging to the studied
183 seismic sequence (Iside database). The integration of such information in a pseudo-3D environment offered us a
184 multidisciplinary platform to clearly display the seismic lines and to link surface data and the deep geologic structures at
185 hypocentral depth.

186 **4 Methods**

187 The seismic reflection data interpretation is generally accomplished through the definition of specific signal characteristics
188 (seismic signature), supported by the geological knowledge of the study area. A standard seismic interpretation is affected by
189 a certain degree of uncertainty/subjectivity (particularly in case of poor data quality), because generally based on a
190 qualitative analysis of reflection amplitude, geometry and lateral continuity. Over the last years, the introduction of seismic
191 attributes and related automated/semi-automated procedures had an important role in reducing the subjectivity of seismic
192 interpretation, at first in 2D/3D seismic reflection data (Barnes 1996; **Taner et al., 1979; Barnes, 1999; Chen and Sidney,**
193 **1997; Taner, 2001; Chopra and Marfurt, 2007; Chopra and Marfurt, 2008; Forte et al., 2016**) and, more recently, also in
194 other reflection techniques like the Ground Penetrating Radar (GPR) (e.g. McClymont et al., 2008; Forte et al., 2012; Ercoli
195 et al., 2015, De Lima et al., 2018). In this work, we have tested several post-stack attributes on three 2D vintage seismic

196 lines, also using composite multi-attribute displays. Among those analysed, we selected the three attributes that resulted in
197 the best images, making possible to detect peculiar seismic signatures of regional seismogenic layers and fault zones. Details
198 about the calculated attributes are hereafter provided.

199
200 **“Energy” (E):** one of the RMS amplitude-based attributes, it is defined as the ratio between the squared sum of the
201 sample values in a specified time-gate and the number of samples in the gate (Taner, 1979, Chopra & Marfurt,
202 2005, Chopra & Marfurt, 2007). The Energy measures the reflectivity in a specified time-gate, so the higher the
203 Energy, the higher is the reflection amplitude. In comparison to the original seismic amplitude, it is independent of
204 the polarity of the seismic data being always positive, and in turn preventing the zero-crossing problems of the
205 seismic amplitude (Forte et al., 2012, Ercoli et al., 2015, Lima et al., 2018, Zhao et al., 2018). This attribute is
206 useful to emphasize the most reflective zones (e.g. characterization of acoustic properties of rocks). It may also
207  enhance sharp lateral variations in seismic events, highlighting discontinuities like fractures and faults. In this work,
208 we set a 20 ms time window (i.e. about the mean wavelet length), obtaining considerable improvements in the
209 visualization of higher acoustic impedance contrasts.

210 **“Energy gradient” (EG):** it is the first derivative of the energy with respect to time (or depth). The algorithm
211 calculates the derivative in moving windows and returns the variation of the calculated energy as a function of time
212 or depth (Chopra & Marfurt, 2007; Forte et al., 2012). It is a simple and robust attribute, also useful for a detailed
213 semi-automatic mapping of horizons with a relative low level of subjectivity. The attribute acts as an edge detection
214 tool, effective in the mapping of the reflection patterns as well as the continuity of both steep discontinuities like
215 faults and fractures, and channels, particularly in slices of 3D data (Chopra & Marfurt, 2007). In this work, we have
216 used the same time window of the Energy, obtaining considerable improvements in the visualization not only of the
217 strong acoustic impedance reflectors but particularly in the faults imaged in the shallowest part of the seismic
218 sections.

219 **Pseudo-relief (PR):** it is obtained in two steps: the energy attribute is first computed in a short time window, then
220 followed by the Hilbert transform (phase rotation of -90 degrees). The Pseudo-relief is considered very useful in 2D
221 seismic interpretation to generate “outcrop-like” images allowing an easier detection of both faults and horizons
222 (Bulhões, 1999; Barnes et al., 2011; Vernengo et al. 2017, Lima et al., 2018). In this work, considerable display
223 improvements have been obtained using the Pseudo-relief computed in a window of 20 ms. In comparison to the
224 standard amplitude, it better highlights the reflection patterns and thus the continuity/discontinuity of reflectors,
225 enhancing steep discontinuities and fault zones.

226 **5 Results**



227 The comparison between the original seismic lines and the images obtained after the attribute analysis allows to detect
228 considerable improvements in the visualization and interpretability of the geophysical features. In profiles NOR01, CAS01

229 and NOR02 (Figs 2, 3 and 4, respectively) we focus our analysis on three main types of geophysical features highlighted by
230 the attributes: sub-horizontal deep reflectors, low-angle and high-angle discontinuities.

231 Analysing in detail the line NOR01 (Fig. 2a, line location in the excerpt on the top), the most apparent low-angle
232 geophysical features are located in the eastern portion of the line between 2-3 s of the time window. The EN attribute in Fig.
233 2b clearly enhances a high-amplitude, gently W-dipping event at about 2.5 s (blue arrows). The EG and SR attributes of
234 NOR01 show clearly that this horizon (Figs. 2c, 2d, hereafter H) is characterized by a continuous package of reflectors (ca.
235 200 ms in TWT, ca. 8 km long), with common characteristics in terms of reflection strength and period.

236 A similar feature showing such a peculiar signature is visible also in CAS01, approximately at the same time interval (Fig.
237 3a, line location reported on the top insert). But in comparison to NOR01, it appears more discontinuous all along the
238 seismic profile, and in addition it is partially interfering with suspicious processing artefacts (highlighted with yellow dots,
239 labelled as “A”, slightly undulated in Fig. 3a whilst horizontal in Fig. 2a ca. at 1 s). For those reasons, H is not particularly
240 clear in the standard amplitude line CAS01 (Fig. 3a), even if it is mainly visible on the westernmost side and beneath the
241 southern termination of Nb (ca. between 11-15 km). Despite a generalized high frequency noise content, H is better
242 enhanced in fig. 3b by EN attribute (blue arrows), and in particular by the EG and PR attributes (Figs. 3c and 3d), that
243 considerably help to better detect and mark its extension and geometry.

244 Regarding the most visible steep geophysical features detectable in these two seismic profiles, in NOR01 a high-angle E-
245 dipping lineament is defined by a clear high-angle discontinuity of the seismic signal, particularly enhanced in the eastern
246 sector (distance ca. 10 km) below the Nb (red arrows in fig. 2c and 2d). A very similar high-angle East-dipping discontinuity
247 can be noticed in the eastern sector of CAS01 (red arrows in Fig. 3c and 3d). Another main high-angle W-dipping lineament
248 is enhanced in Figs. 2c-2d of NOR01 (red arrows at the end of the line), that clearly divides two patterns of reflectors
249 showing different dip; this discontinuity propagates down to ca. 2.5 s and intercepts the aforementioned strong reflector H.
250 Between those two main alignments bounding the Nb, other similar but minor discontinuities can be also noticed crossing
251 and slightly disrupting the shallower reflectors: those high angle features are efficiently displayed by the EG and PR
252 attributes (Fig. 2c, 2d), whilst in the original line in Fig. 2a cannot be really appreciated.

253 The figure 4a display the original seismic line NOR02 characterized by similar geophysical features (location on the top
254 insert). The EN attribute in Fig. 4b again results efficient in enhancing sub-horizontal (blue arrows) and also gently dipping
255 deep events (green dots). On the western sector, the attributes in Figs. 4b and 4c show a pattern of relatively continuous and
256 gently W-dipping events between 0-2.5 s (0-5 km along the line). The most evident high-amplitude and continuous reflector
257 characterizes the central part of NOR02 at ca. 3.2–3.5 s (blue arrows in Figs. 4b, 4c, 4d), gently East-dipping and relatively
258 continuous for more than 8 km. This latter is intercepted by an important and well visible low-angle W-dipping discontinuity
259 (T, green dots in Figs. 4b, 4c and 4d). It crosses the entire profile, rising from about 4 s (West) to ca. 2 s (East), where it
260 intercepts one of the high amplitude events on the eastern end of the seismic line (18-20 km). Here again the attribute
261 analysis results extremely efficient to clearly detect such geophysical features otherwise poorly visible on the original line
262 NOR02 in Fig. 4a.

263 The most important result provided by the EG and PR attributes is a much clear visualization of the reflection patterns of
264 NOR02, aiding an easier detection of high-angle discontinuities, at different scales. In fact, a main high-angle E-dipping
265 discontinuity (red arrows) delimits the NOR02 western sector (ca. 1 km of distance along the line at surface); another steep
266 W-dipping alignment (red arrows) clearly cuts and slightly disrupt the set of reflectors below the Nb (0-2.5 s, ca. 4-5 km). In
267 addition, smaller discontinuities pervasively cross-cut the set of reflectors between 1-4 km bounded by such two main
268 features, producing a densely fragmented reflectors pattern in the middle portion. Another steep E-dipping feature is visible
269 at higher depth (red arrows at 1-3 s, ca. 7-9 km) beneath the topographic relief separating Nb by CNb: it seems to end up on
270 the deep surface T and in addition it doesn't reach the shallower portion of the seismic line. This discontinuity is subparallel
271 to a similar structure displayed in a more central portion of NOR02 (western side of CNb highlighted by red arrows at 10-12
272 km). The Figs. 4c and 4d show here sets of reflectors sharply interrupted, fragmented and displaced in a narrow zone. The
273 same seismic pattern is present in the western side of CNb, but it is due to some west-dipping discontinuities located
274 between 14-16 km. These features highlight an asymmetric "V-shape" fabric characterized by very short and fragmented
275 reflectors bounded by those two steep features of opposite dip. The deep continuation of such a main W-dipping alignment
276 also seems to truncate and disrupt both the gently-dipping discontinuity T and the deep reflector H: at approximately 3.2 s, it
277 appears interrupted laterally on its western side (Figs. 4c and 4d).

278 The results of this work produced has globally improved the interpretability of the original dataset. In particular, the data
279 integration in a 3D environment and the use of multi-attribute displays clarified the deep geometries of the main reflectors
280 and of the geophysical discontinuities, later interpreted on the light of the known and debated tectonic structures on the study
281 area. This is particularly clear in Fig. 5a, in which we report the seismic line NOR02 after the combined plot of the PR
282 attribute ("similarity" palette) with superimposed the EG attribute ("energy" palette), overlapped using ODT software (depth
283 conversion with $V_{pav} = 6000$ m/s, vertical scale 2x). The reflectors characteristics and the discontinuities are clearly visible at
284 different levels of detail, and the two boxes (blue and black colours, respectively) highlight on the two most representative
285 seismic facies described before. The blue box of Fig.5a is reported in Fig. 5b and 5c by displaying a comparison of the H
286 signature in the original line and a plot of the EN attribute superimposed on the PR attribute. On the two other inserts in Figs.
287 5d and 5e, the same comparison of the data included in the black box is proposed. Fig.4d shows the scarce detectability of
288 the dense pattern of steep discontinuities in the original seismic profile (SA). The Fig.5e displays the enhancement obtained
289 plotting the PR attribute ("similarity palette") in transparency on the seismic line in amplitude (SA).

290 An analogous visualization is proposed in Fig. 6a for the seismic line NOR01. The comparison between the multi-display of
291 attributes PR and EG (blue box in Fig. 6a), the original line (Fig. 6b) and the EN+PR plot (Fig.6c) shows the improved
292 signature of the strong reflector H. The black box again reports the original line NOR01 and the version PR+SA, clearly
293 boosting the visualization of the high-angle discontinuities.

294 Such results therefore ensure an easier and more accurate interpretation of the subsurface geological structures; those are
295 connected with the surface geology and related to the hypocentre location of the main seismic events, that will be discussed
296 more in detail within the following chapter.

297 6 New constraints on the deep geological structure reconstruction

298 Due to the lack of 3D seismic volumes and of a regular grid of 2D seismic profiles in the area, the geological meaning of the
299 results provided by the attributes analysis have been constrained by integrating all the other available literature data. We
300 have therefore integrated geological and structural maps (Koopman, 1983; Centamore et al., 1993; Pierantoni et al., 2013),
301 high-resolution topographic data (Tarquini et al., 2007 and 2012), mainshocks hypocentral data (Chiaraluca et al., 2017) and
302 co-seismic surface ruptures data (Civico et al., 2018; Villani et al., 2018; Brozzetti et al., 2019).

303 In fig. 7, a 3D overview of the study region summarizes the data analysed across the area surrounding the Mw 6.5 mainshock
304 (30th October 2016), plotted together with other three strong seismic events in the Northern sector. The two seismic images
305 in Figs. 7b and 7c have been obtained by using again a multi-attributes visualization, in this case overlapping the PR and EN
306 attributes in transparency with the original seismic lines NOR01 and NOR02. The black boxes centred on the NB and CNb
307 basins have been magnified above and display the limits of the bounding faults (black dashed lines) and the main important
308 reflectors detected in depth. In the Figs. 7d and 7e, we propose a detailed interpretation of the geophysical features displayed
309 by the attribute images, together with the location of the focal mechanisms of the principal mainshocks.

310 The deep, high-amplitude reflector (H, blue arrows and dashed line) highlighted to the West of Nb in NOR01 (at 2.5 s, in
311 Figs. 2d and 7d and in Figs. 3d of CAS01), presents an attribute signature similar to the one deeper visible in NOR02
312 beneath CNb (3.2 s, in Figs. 4b and 7e). This set of reflectors are interpreted as a high acoustic impedance contrast, possibly
313 related to an important velocity inversion occurring between the Triassic Evaporites (anhydrites and dolostones, $V_p \approx 6$
314 km/s, e.g. Trippetta et al., 2010) and the underlying acoustic Basement (metasedimentary rocks, $V_p \approx 5$ km/s, sensu Bally et
315 al., 1986). Similar, prominent reflections were detected in adjacent regions of the Umbria-Marche Apennines (e.g. Mirabella
316 et al., 2008) confirming its regional importance, particularly because it represents a lithological control marking a seismicity
317 cutoff (Porreca et al., 2018; Mancinelli et al., 2019).

318 The continuity of the deep reflector H is interrupted in the western edge by the low-angle west-dipping T discontinuity
319 crossing NOR02 (Figs. 4d and 7e), not identified by Porreca et al. (2018). We interpret this discontinuity as the evidence of a
320 deep thrust emerging in the easternmost sector of the region.

321 The steep discontinuities highlighted by the attribute analysis are here interpreted as the seismic signature at depth of
322 complex normal faults mapped at the surface. More in detail, the most evident seismic discontinuity is marked by an E-
323 dipping fault in NOR01, bordering westward the Nb (Figs. 2d and 7d). The latter does not have a clear surface expression
324 and therefore its presence is still debated in literature (Blumetti et al., 1993; Pizzi et al., 2002; Galadini et al., 2018; Galli et
325 al., 2018): its location and geometry in NOR01 perfectly match the supposed position at surface. Therefore, it may represent
326 the evidence of the antithetic normal fault of Norcia (aNf), belonging to a conjugate tectonic system (Brozzetti & Lavecchia,
327 1994; Lavecchia et al., 1994) and suggested by morphological evidences (Blumetti et al., 1990) and paleoseismological
328 records (Borre et al., 2003). It is a synthetic (W-dipping) high-angle, normal fault bordering the eastern flank of Nb
329 (“Nottoria-Preci fault” – Nf, Calamita et al., 1982; Blumetti et al., 1993; Calamita & Pizzi, 1994). The Nf in NOR02 is

330 evident by a downward propagation of steep alignments (red arrows, Figs. 2c, 2d and 7d), that generates sharp lateral
331 truncations of the gently W-dipping reflectors. This area is also fragmented by several minor strands parallel to the main
332 faults (Figs. 7d). In addition, another similar structure is visible slightly eastward (Figs. 4c, 4d red arrows between 7-9 km,
333 ca. 1-3 s and westernmost dashed black line in Fig. 7e). It is not reaching the shallower portion of the seismic line, but it is
334 clearly visible in depth down to the discontinuity T. This feature might be interpreted as a parallel E-dipping fault, moreover
335 suggested by several authors to be connected with an aftershock (Mw5.4), that “ruptured a buried antithetic normal fault on
336 eastern side of Nb, parallel to the western bounding fault of CNb” (Chiaraluce et al., 2017, Porreca et al., 2018 and Improta
337 et al., 2019).

338 The central sector of NOR02 including CNb, was described as a “triangle-shaped zone” by Porreca et al. (2018), who remark
339 a generalized difficulty to detect the accurate position of the normal faults. The multi-attribute visualization shows a clear
340 reflection fabric dominated by high-angle discontinuities. Those are interpretable as two opposite dipping normal faults
341 bordering the basin, well matching their positions mapped at surface (cfr. Pierantoni et al., 2013).

342 The main fault is here represented by the W-dipping Vf fault, reactivated during the 2016 earthquake (Villani et al., 2018a).
343 It can be traced, from its surface expression downward to hypocentre location along its deep seismic signature, made by
344 several high-angle seismic discontinuities cross-cutting the gently W-dipping reflectors (Figs. 4d and 7e). At depth, the Vf
345 seems also to displace the Top Basement (H) and the thrust (T) at about 3.2 s.

346 Analogous considerations can be extended to the E-dipping set of steep events at the westward side of CNb. These may
347 represent evidence of an antithetic fault (aVf), made by several minor fault strands (Villani et al., 2018b). Such a fault
348 appears connected at about 2-3 s to the W-dipping master Vf, producing a geometry of a conjugate system similar to Nb
349 (Figs. 4d and 7e).

350 For both Nb and CNb, the interpreted data suggest two slightly asymmetric fault systems, due to conjugate sets of
351 seismogenic master faults (Ramsay & Huber, 1987) producing a “basin-and-range” morphology (Serva et al., 2002). Those
352 control the evolution of the continental basins, and are associated with several complex sets of secondary strands, able to
353 produce surface ruptures as occurred in the 2016-2017 seismic swarm.

354 The attribute images produced in this work suggest that such synthetic and antithetic tectonic structures at the Nb and CNb
355 cannot be actually simplified as a unique fault plane, but as complex and fractured fault zones (Fz, in Fig. 7d), like also
356 conceived also by Ferrario & Livio (2018) as “distributed faulting and rupture zones”.

357 **Conclusions**

358 Taking into account the important role that seismic attributes play in the O&G industry their usage might be similar interest
359 for seismotectonic studies. And have a high potential impact on earthquakes hazard assessment.

360 This contribution presents one of the first case studies where the seismic attribute analysis is used for seismotectonic purposes.

361 The analysis is applied to seismic reflection data collected more than 30 years ago in Central Italy. Such industrial data,

362 nowadays irreproducible in regions where the seismic exploration is forbidden, represent, despite the limited quality, a unique
363 high-resolution source of information.

364 This contribution reveals that the use of seismic attributes can ~~greatly~~ improve the interpretation for the subsurface assessment
365 and structural characterization. Certainly, the overall low quality of the data sets did neither allow to extract rock petrophysical
366 parameters, nor more quantitative information. However, the attributes aid the seismic interpretation to better display the
367 reflection patterns of interest and provided new and original details on complex tectonic region in Central Italy. We
368 considerably improved the overall interpretability of the vintage seismic lines crossing the epicentral area of the 2016-2017
369 Norcia-Amatrice seismic sequence. In particular, we detected peculiar seismic signatures of a deep horizon of regional
370 importance, corresponding, most probably, to the base of the seismogenic layer, and to the location and geometry of the
371 complex active fault zones. Those consists of several secondary synthetic and antithetic splays in both the Quaternary basins,
372 generally consistent with its surface location, but also reinforcing the existence of faults with no clear surface outcrop, issue
373 currently much debated in the literature.

374 The analysis and integration of the seismic attributes has allowed the determination of the deep continuation of the (known
375 and supposed) faults and, the recently mapped co-seismic ruptures at surface, providing a pseudo-3D picture of the buried
376 structural setting of the area. The seismic attributes may help to reduce the gap between the surface geology and deep
377 seismological data, also revealing, a high structural complexity at different scales, that cannot generally be detected by using
378 only traditional interpretation techniques. This approach has shown the potential of the attributes analysis , that even when
379 applied on 2D vintage seismic lines, may significantly extend the data value. For all these reasons, we strongly encourage its
380 application for seismotectonic research to provide new information and additional constraints across other seismically active
381 regions around the world.

382 **Acknowledgments**

383 We are grateful to Eni S.p.A. for providing an inedited set of seismic reflection lines after the 2016-2017 seismic crisis in
384 Central Italy (raw data available in Fig.2 of supporting information). The original seismic reflection lines used in this study
385 are available in the supplementary material. The authors are very grateful to dgB Earth Sciences and to QGIS team for
386 providing the academic software used in this work. We thank Dr. Christian Berndt for his useful comments in the revision of
387 the paper.

- 389 Allen, C. R., St. Amand, P., Richter, C. F., & Nordquist, J.: Relationship between seismicity and geologic structure in the
390 southern California region. *Bulletin of the Seismological Society of America*, 55(4), 753-797, 1965.
- 391 Anelli, L., Gorza, M., Pieri, M., and Riva, M.: Subsurface well data in the Northern Apennines (Italy). *Memorie della Società*
392 *Geologica Italiana*, 48, 461–471, 1994.
- 393 Bally, A. W., Burbi, L., Cooper, C., & Ghelardoni, R.: Balanced cross-sections and seismic reflection profiles across the central
394 Apennines. *Memorie della Società Geologica Italiana*, 35, 257–310, 1986.
- 395 Barchi, M.: Integration of a seismic profile with surface and subsurface geology in a cross-section through the Umbria-Marche
396 Apennines. *Bollettino della Società Geologica Italiana*, 110, 469–479, 1991.
- 397 Barchi, M. R., Minelli, G. and Pialli, G.: The CROP 03 Profile: a synthesis of results on deep structures of the Northern
398 Apennines, *Mem. Soc. Geol. It.*, 52, 383-400, 1998.
- 399 Barchi M.R., Galadini, F., Lavecchia, G., Messina, P., Michetti, A. M., Peruzza, L., Pizzi, A., Tondi & Vittori, E.: Sintesi delle
400 conoscenze sulle faglie attive in Italia Centrale: parametrizzazione ai fini della caratterizzazione della pericolosità sismica.
401 CNR-Gruppo Nazionale per la Difesa dai Terremoti, Roma, 62 pp., 2000.
- 402 Barchi, M., Landuzzi, A., Minelli, G., & Pialli, G.: Outer northern Apennines. In *anatomy of an orogen: The Apennines and*
403 *adjacent Mediterranean Basins*. Netherlands, Springer, 215–253, 2001.
- 404 Barchi, M. R., & Mirabella, F.: The 1997-98 Umbria-Marche earthquake sequence: “Geological” vs. “seismological” faults.
405 *Tectonophysics*, 476(1–2), 170–179. <https://doi.org/10.1016/j.tecto.2008.09.013>, 2009.
- 406 Barnes, A. E.: Theory of two-dimensional complex seismic trace analysis. *Geophysics*, 61, 264–272, 1996.
- 407 Barnes, A. E.: Attributes for automating seismic facies analysis. *SEG Technical Program Expanded Abstracts*, 19.
408 doi:10.1190/1.1816121, 1999.
- 409 Barnes, A. E.: "Displaying Seismic Data to Look Like Geology", chapter of: “Attributes: New Views on Seismic Imaging–
410 Their Use in Exploration and Production”, Marfurt, K. J. Gao, D., Barnes, A., Chopra, S., Corrao, A., Hart, B., James, H.,
411 Pacht, J., Rosen, N.C. (2011), *SEPM Society for Sedimentary Geology*, 31, doi: 10.5724/ges.11.31, 2011.
- 412 Barnes, A., E.: *Handbook of Poststack Seismic Attributes*, Society of Exploration Geophysicists, 21, doi:
413 10.1190/1.9781560803324, 2016.
- 414 Basili, R., Valensise, G., Vannoli, P., Burrato, P., Fracassi, U., Mariano, S., ... & Boschi, E.: The Database of Individual
415 Seismogenic Sources (DISS), version 3: summarizing 20 years of research on Italy's earthquake geology. *Tectonophysics*,
416 453(1-4), 20-43, 2008.
- 417 Beidinger, A., Decker, K., & Roch, K. H.: The Lasse segment of the Vienna Basin fault system as a potential source of the
418 earthquake of Carnuntum in the fourth century AD. *International Journal of Earth Sciences*, 100(6), 1315-1329, 2011.
- 419 Bigi, S., Casero, P., & Ciotoli, G.: Seismic interpretation of the Laga basin; constraints on the structural setting and kinematics
420 of the central Apennines. *Journal of the Geological Society*, 168(1), 179–190. doi 10.1144/0016-76492010-084, 2011.

421 Borre, K., Cacon, S., Cello, G., Kontny, B., Likke Andersen, H., Moratti, G., Piccardi, L., Stemberk, J., Tondi, E., Vilimek,
422 V.: The COST project in Italy: analysis and monitoring of seismogenic faults in the Gargano and Norcia areas (centralsouthern
423 Apennines, Italy). *J. Geodyn.* 36, 3 –18, 2003.

424 Blumetti, A.M., Coltorti, M., Dramis, F., Farabollini, P.: Due sezioni stratigrafiche nel Pleistocene medio della conca di Norcia;
425 implicazioni geomorfologiche e neotettoniche. *Rend. Soc. Geol. Ital.* 13, 17– 26, 1990.

426 Blumetti, A. M., Dramis, F., & Michetti, A. M.: Fault-generated mountain fronts in the central Apennines (Central Italy):
427 Geomorphological features and seismotectonic implications. *Earth Surface Processes and Landforms*, 18(3), 203–223. doi:
428 10.1002/esp.3290180304, 1993.

429 Bonini, L., Toscani, G., & Seno, S.: Three-dimensional segmentation and different rupture behavior during the 2012 Emilia
430 seismic sequence (Northern Italy). *Tectonophysics*, 630, 33-42, 2014.

431 Bonini, L., Basili, R., Burrato, P., Cannelli, V., Fracassi, U., Maesano, F. E., et al.: Testing different tectonic models for the
432 source of the Mw 6.5, 30 October 2016, Norcia earthquake (central Italy): A youthful normal fault, or negative inversion of
433 an old thrust? *Tectonics*, 38, doi:10.1029/2018TC005185, 2019.

434 Boncio, P., F. Brozzetti, and G. Lavecchia: Architecture and seismotectonics of a regional low-angle normal fault zone in
435 central Italy, *Tectonics*, 19(6), 1038–1055, doi:10.1029/2000TC900023, 2000.

436 Boncio, P., Lavecchia, G., & Pace, B.: Defining a model of 3D seismogenic sources for seismic hazard assessment applications:
437 The case of central Apennines (Italy). *Journal of Seismology*, 8(3), 407–425, 2004.

438 Brewer, J. A., Matthews, D. H., Warner, M. R., Hall, J., Smythe, D. K., & Whittington, R. J.: BIRPS deep seismic reflection
439 studies of the British Caledonides. *Nature*, 305(5931), 206, 1983.

440 Brozzetti, F., & Lavecchia, G.: Seismicity and related extensional stress field: the case of the Norcia seismic zone. *Annales*
441 *Tectonicae*, 8, 38–57, 1994.

442 Brozzetti, F., Boncio, P., Cirillo, D., Ferrarini, F., de Nardis, R., Testa, A., Liberi, F., & Lavecchia, G.: High resolution field
443 mapping and analysis of the August – October 2016 coseismic surface faulting (Central Italy Earthquakes): slip distribution,
444 parameterization and comparison with global earthquakes. *Tectonics*, 38. <https://doi.org/10.1029/2018TC005305>, 2019.

445 Bulhões, E.M.: Técnica “Volume de Amplitudes”. SBGF/6° Congresso Internacional da Sociedade Brasileira de Geofísica,
446 Rio de Janeiro, Anais (In Portuguese), 1999.

447 Calamita, F., Coltorti, M., Deiana, G., Dramis, F. and Pambianchi, G.: Neotectonic evolution and geomorphology of the Cascia
448 and Norcia depressions (Umbria-Marche Apennines), *Geografia Fisica e Dinamica Quaternaria*, 5, 263-276, 1982.

449 Calamita, F., & Pizzi, A.: Recent and active extensional tectonics in the southern Umbro-Marchean Apennines (Central Italy).
450 *Memorie della Società Geologica Italiana*, 48, 541–548, 1994.

451 Calamita, F., Pace, P., & Satolli, S., Coexistence of fault-propagation and fault-bend folding in curve-shaped foreland fold-
452 and-thrust belts: examples from the Northern Apennines (Italy). *Terra Nova*, 24(5), 396-406, 2012.

453 Carvalho, J., Taha, R., Cabral, J., Carrilho, F. and Miranda, M.: Geophysical characterization of the OtaVila Franca de Xira-
454 Lisbon-Sesimbra fault zone, Portugal. *Geophysical Journal International*, 174, 567-584, 2008.

455 Cavinato, G. P., & De Celles, P. G.: Extensional basins in the tectonically bimodal central Apennines fold-thrust belt, Italy:
456 Response to corner flow above a subducting slab in retrograde motion. *Geology*, 27(10), 955–958, 1999.

457 Centamore, E., Adamoli, L., Berti, D., Bigi, G., Bigi, S., Casnedi, R., et al.: Carta geologica dei bacini della Laga e del Cellino
458 e dei rilievi carbonatici circostanti. In: *Studi Geologici Camerti*, Vol. Spec. Università degli Studi, Dipartimento di Scienze
459 della Terra. SELCA, Firenze, 1992.

460 Cheloni, D., Falcucci, E., & Gori, S.: Half-graben rupture geometry of the 30 October 2016 MW 6.6 Mt. Vettore-Mt. Bove
461 earthquake, central Italy. *Journal of Geophysical Research: Solid Earth*, 124. <https://doi.org/10.1029/2018JB015851>

462 Chen, Q. and Sidney, S.: Seismic Attribute Technology for Reservoir Forecasting and Monitoring. *The Leading Edge*, 16 (5):
463 445. <http://dx.doi.org/10.1190/1.1437657>, 1997.

464 Chiarabba, C., De Gori, P., Cattaneo, M., Spallarossa, D., & Segou, M.: Faults geometry and the role of fluids in the 2016–
465 2017 Central Italy seismic sequence. *Geophysical Research Letters*, 45, 6963–6971, 2018.

466 Chiaraluca, L., Barchi, M., Collettini, C., Mirabella, F. & Pucci, S. Connecting seismically active normal faults with
467 Quaternary geological structures in a complex extensional environment: the Colfiorito 1997 case history (northern Apennines,
468 Italy). *Tectonics* 24, TC1002, <https://doi.org/10.1029/2004TC001627>, 2005.

469 Chiaraluca, L., Di Stefano, R., Tinti, E., Scognamiglio, L., Michele, M., Casarotti, E., et al.: The 2016 Central Italy seismic
470 sequence: A first look at the mainshocks, aftershocks, and source models. *Seismological Research Letters*, 88(3), 757–771.
471 <https://doi.org/10.1785/0220160221>, 2017.

472 Chopra, S. & J. Marfurt, K.: Seismic attributes - A Historical Perspective. *Geophysics*. 70(5):3.
473 <https://doi.org/10.1190/1.2098670>, 2005.

474 Chopra, S. and Marfurt, K. J.: *Seismic Attributes for Prospect Identification and Reservoir Characterization*. SEG Geophysical
475 Developments Series No. 11, Stephen J. Hill, series editor and volume editor. ISBN 978-1-56080-141-2 (volume) - ISBN 978-
476 0-931830-41-9 (series), 464 pp, 2007.

477 Chopra, S. & J. Marfurt, K.: Emerging and future trends in seismic attributes. *The Leading Edge*. 27. 298-318.
478 [10.1190/1.2896620](https://doi.org/10.1190/1.2896620), 2008.

479 Ciaccio, M., Barchi M. R., Chiarabba, C., Mirabella, F. and Stucchi E.: Seismological, geological and geophysical constraints
480 for the Gualdo Tadino fault, Umbria-Marche Apennines (central Italy), *Tectonophysics*, 406, 233 – 247, 2005.

481 Civico, R., Pucci, S., Villani, F., Pizzimenti, L., De Martini, P. M., Nappi, R. & the Open EMERGEO Working Group: Surface
482 ruptures following the 30 October 2016 Mw 6.5 Norcia earthquake, central Italy, *Journal of Maps*, 14:2, 151-160, doi:
483 [10.1080/17445647.2018.1441756](https://doi.org/10.1080/17445647.2018.1441756), 2018.

484 Coltorti, M., Farabollini, P.: Quaternary evolution of the “Castelluccio di Norcia” basin (Umbro-Marchean Apennines, central
485 Italy). *Il Quaternario* 8(1), 149–166, 1995.

486 Cook, F. A., Albaugh, D. S., Brown, L. D., Kaufman, S., Oliver, J. E., & Hatcher Jr, R. D.: Thin-skinned tectonics in the
487 crystalline southern Appalachians; COCORP seismic-reflection profiling of the Blue Ridge and Piedmont. *Geology*, 7(12),
488 563-567, 1979.

489 De Guidi, G., Vecchio, A., Brighenti, F., Caputo, R., Carnemolla, F., Di Pietro, A., et al.: Co-seismic displacement on October
490 26 and 30, 2016 (Mw 5.9 and 6.5) earthquakes in central Italy from the analysis of discrete GNSS network. *Natural Hazards*
491 *and Earth System Sciences Discussions*, 2017(May), 1–11. doi: 10.5194/nhess-2017-130, 2017.

492 Deschamps, A., Innaccone, G., & Scarpa, R.: The Umbrian earthquake (Italy) of 19 September 1979. *Annales Geophysicae*,
493 2, 29–36, 1984.

494 De Lima, R. & Luiz Evangelista Teixeira, W. & Ramos de Albuquerque, F. & Lima-Filho, F. P.: Ground Penetrating Radar
495 digital imaging and modeling of microbialites from the Salitre Formation, Northeast Brazil. *Geologia USP - Serie Cientifica*,
496 18, 187-200. doi: 10.11606/issn.2316-9095.v18-146075, 2018.

497 Di, H., and AlRegib, G.: Semi-automatic fault/fracture interpretation based on seismic geometry analysis: Geophysical
498 Prospecting, doi: 10.1111/1365-2478.12769, 2019.

499 DISS Working Group: Database of Individual Seismogenic Sources (DISS), Version 3.2.1: A compilation of potential sources
500 for earthquakes larger than M 5.5 in Italy and surrounding areas. <http://diss.rm.ingv.it/diss/>, Istituto Nazionale di Geofisica e
501 Vulcanologia, doi: 10.6092/INGV.IT-DISS3.2.1, 2018.

502 Ercoli, M., Pauselli, C., Frigeri, A., Forte, E., & Federico, C.: “Geophysical paleoseismology” through high resolution GPR
503 data: A case of shallow faulting imaging in Central Italy. *Journal of Applied Geophysics*, 90, 27–40.
504 doi.org/10.1016/j.jappgeo.2012.12.001, 2013.

505 Ercoli M., Pauselli C., Frigeri A., Forte E. and Federico C.: 3-D GPR data analysis for high-resolution imaging of shallow
506 subsurface faults: the Mt Vettore case study (Central Apennines, Italy). *Geophysical Journal International*, 198:1(609-621).
507 doi: 10.1093/gji/ggu156, 2014.

508 Ercoli, M., Pauselli, C., Cinti, F.R., Forte, E. and Volpe, R.: Imaging of an active fault: Comparison between 3D GPR data
509 and outcrops at the Castrovallari fault, Calabria, Italy. *Interpretation*, 3(3), pp. SY57-SY66, 2015.

510 Ferrario, M. F., & Livio, F.: Characterizing the distributed faulting during the 30 October 2016, Central Italy earthquake: A
511 reference for fault displacement hazard assessment. *Tectonics*, 37, 1256–1273. <https://doi.org/10.1029/2017TC004935>, 2018.

512 Finetti, I. R., Boccaletti, M., Bonini, M., Del Ben, A., Geletti, R., Pipan, M., & Sani, F.: Crustal section based on CROP seismic
513 data across the North Tyrrhenian–Northern Apennines–Adriatic Sea. *Tectonophysics*, 343(3-4), 135-163, 2001.

514 Ferrario, M. F., & Livio, F.: Characterizing the distributed faulting during the 30 October 2016, Central Italy earthquake: A
515 reference for fault displacement hazard assessment. *Tectonics*, 37. doi:10.1029/2017TC004935, 2018.

516 Forte E., Pipan M., Casabianca D., Di Cuia R., Riva A.: Imaging and characterization of a carbonate hydrocarbon reservoir
517 analogue using GPR attributes. *Journal of Applied Geophysics*, 81, 76–87, 2012.

518 Forte E., Dossi M., Pipan M. and Del Ben A.: Automated phase attribute-based picking applied to reflection seismics,
519 *Geophysics*, 81, 2, V55-V64, doi: 10.1190/GEO2015-0333.1, 2016.

520 Galadini, F., & Galli, P.: Paleoseismology of silent faults in the central Apennines (Italy): The Mt. Vettore and Laga Mts.
521 Faults. *Annals of Geophysics*, 46. <https://doi.org/10.4401/ag-3457>, 2003.

522 Galadini, F., Falcucci, E., Gori, S., Zimmaro, P., Cheloni, D. and Stewart J. P.: Active Faulting in Source Region of 2016–
523 2017 Central Italy Event Sequence. *Earthquake Spectra*, 34, 4, 1557-1583, 2018.

524 Galli, P., Galadini, F., Calzoni, F.: Surface faulting in Norcia (Central Italy): a “paleoseismological perspective”.
525 *Tectonophysics*, 403, 117–130, 2005.

526 Galli, P., Galadini, F. & Pantosti, D.: Twenty years of paleoseismology in Italy, *Earth-Sci. Rev.*, 88(1–2), 89–117, 2008.

527 Galli, P., Galderisi, A., Iardo, I., Piscitelli, S., Scionti, V., Bellanova, J., Calzoni, F.: Holocene paleoseismology of the Norcia
528 fault system (Central Italy), *Tectonophysics*, 745, 154-169, doi:10.1016/j.tecto.2018.08.008, 2018.

529 Gruppo di Lavoro Sequenza Centro Italia: Rapporto Bollettino Sismico Italiano sulla revisione dei giorni 24-26 agosto; 26-27
530 ottobre; 30 ottobre - 1° novembre 2016. *Bollettino Sismico Italiano (BSI)*, 13 pp., 2019.

531 Jibson, R.W., Allstadt, K.E., Rengers, F.K., and Godt, J.W.: Overview of the geologic effects of the November 14, 2016, Mw
532 7.8 Kaikoura, New Zealand earthquake, U.S. Geological Survey Scientific Investigations Report, 2017–5146, 39 pp.,
533 <https://doi.org/10.3133/sir20175146>, 2018.

534 Ha, T. N., Marfurt, K. J. and Wallet B. C., Hutchinson, B.: Pitfalls and implementation of data conditioning, attribute analysis,
535 and self-organizing mapping to 2D data: Application to the Exmouth Plateau, North Carnarvon Basin, Australia, Interpretation,
536 submitted, http://mcee.ou.edu/aaspi/submitted/2019/Ha_et_al_2019_Seismic_attributes_for_2D_data.pdf, 2019.

537 Hale, D.: Methods to compute fault images, extract fault surfaces, and estimate fault throws from 3D seismic images.
538 *Geophysics*, 78(2), O33–O43, <https://doi.org/10.1190/geo2012-0331.1>, 2013.

539 Hutchinson, B.: Application and Limitations of Seismic Attributes on 2D Reconnaissance Surveys: Master’s thesis, University
540 of Oklahoma, 130 pp., 2016. <https://shareok.org/handle/11244/34658>.

541 Improta, L., Latorre, D., Margheriti, L., Nardi, A., Marchetti, A., Lombardi, A. M., Castello, B., Villani, F., Ciaccio, M. G.,
542 Mele, F. M., Moretti, M. & the Bollettino sismico Italiano Working Group: Multi-segment rupture of the 2016 Amatrice-
543 Visso-Norcia seismic sequence (central Italy) constrained by the first high-quality catalog of early Aftershocks. *Scientific*
544 *Reports*, 9, 6921, 2019. doi: 10.1038/s41598-019-43393-2

545 ISIDe working group: version 1.0; doi:10.13127/ISIDe, 2016.

546 Ithaca catalogue, Available at: [http://www.isprambiente.gov.it/it/progetti/ suolo-e-territorio-1/ithaca-catalogo-delle-faglie-](http://www.isprambiente.gov.it/it/progetti/suolo-e-territorio-1/ithaca-catalogo-delle-faglie-capaci)
547 [capaci](http://www.isprambiente.gov.it/it/progetti/suolo-e-territorio-1/ithaca-catalogo-delle-faglie-capaci), last accessed January 2019.

548 Koopman, A.: Detachment tectonics in the central Apennines, Italy. *Geologica Eltraiectina*, 30, 1–155, 1983.

549 Lavecchia, G.: Il sovrascorrimento dei Monti Sibillini: Analisi cinematica e strutturale. *Bollettino della Società Geologica*
550 *Italiana*, 104, 161–194, 1985.

551 Lavecchia, G., Brozzetti, F., Barchi, M., Keller, J., & Menichetti, M.: Seismotectonic zoning in east-central Italy deduced from
552 the analysis of the Neogene to present deformations and related stress fields. *Geological Society of America Bulletin*, 106,
553 1107–1120, 1994.

554 Lavecchia, G., Castaldo, R., de Nardis, R., De Novellis, V., Ferrarini, F., Pepe, S., Brozzetti, F., Solaro, G., Cirillo, D., Bonano,
555 M., Boncio, P., Casu, F., De Luca, C., Lanari, R., Manunta, M., Manzo, M., Pepe, A., Zinno, I., Tizzani, P.: Ground

556 deformation and source geometry of the 24 August 2016 Amatrice earthquake (Central Italy) investigated through analytical
557 and numerical modeling of DInSAR measurements and structural-geological data. *Geophysical Research Letters*, 43, 12,389–
558 12,398 American Geophysical Union (AGU), 2016.

559 Lima, R. & Teixeira, L. E. W., de Albuquerque, F. R., and Lima-Filho, F. (2018). Ground Penetrating Radar digital imaging
560 and modeling of microbialites from the Salitre Formation, Northeast Brazil. *Geologia USP - Serie Cientifica*. 18. 187-200.
561 10.11606/issn.2316-9095.v18-146075.

562 Livio, F., Michetti, A. M., Vittori, E., Gregory, L., Wedmore, L., Piccardi, L., et al.: Surface faulting during the August 24,
563 2016, central Italy earthquake (Mw 6.0): Preliminary results. *Annals of Geophysics*, 59. doi: 10.4401/ag-7197, 2016.

564 Maesano, F. E., D'Ambrogi, C., Burrato, P., & Toscani, G.: Slip-rates of blind thrusts in slow deforming areas: examples from
565 the Po Plain (Italy). *Tectonophysics*, 643, 8-25, 2015.

566 Mancinelli, P., Porreca, M., Pauselli, C., Minelli, G., Barchi, M. R., & Speranza, F.: Gravity and magnetic modeling of Central
567 Italy: Insights into the depth extent of the seismogenic layer. *Geochemistry, Geophysics, Geosystems*, 20, 2019,
568 <https://doi.org/10.1029/2018GC008002>.

569 Marfurt, K. J. Gao, D., Barnes, A., Chopra, S., Corrao, A., Hart, B., James, H., Pacht, J., Rosen, N.C.: SEPM Society for
570 Sedimentary Geology, 31, doi: 10.5724/gcs.11.31, 2011.

571 Marfurt, K. J.: Seismic Attributes as the Framework for Data Integration throughout the Oilfield Life Cycle, SEG, 508 pp.,
572 2018.

573 Martinis, B., and Pieri, M.: Alcune notizie sulla formazione evaporitica dell'Italia centrale e meridionale. *Bollettino della*
574 *Società Entomologica Italiana*, 4, 649–678, 1964.

575 Mazzotti, A., Stucchi, E., Fradelizio, G., Zanzi, L., Scandone, P.: Seismic exploration in complex terrains: A processing
576 experience in the southern Apennines. *Geophysics*, 65(5), 1402–1417. <https://doi.org/10.1190/1.1444830>, 2000.

577 McClymont, A. F., Green, A. G., Villamor, P., Horstmeyer, H., Grass, C. and Nobes, D. C.: Characterization of the shallow
578 structures of active fault zones using 3-D ground-penetrating radar data, *J. Geophys. Res.*, 113, B10315,
579 doi:10.1029/2007JB005402, 2008.

580 Milli, S., Moscatelli, M., Stanzione, O., & Falcini, F.: Sedimentology and physical stratigraphy of the Messinian turbidites
581 deposits of the Laga basin (Central Apennines, Italy). *Bollettino della Società Geologica Italiana*, 126, 37–48, 2007.

582 Minelli, G., and Menichetti, M.: Tectonic evolution of the Perugia massifs area (Central Italy). *Bollettino della Società*
583 *Entomologica Italiana*, 109(5), 445–453, 1990.

584 Mirabella, F., Barchi, M. R. and Lupattelli, A.: Seismic reflection data in the Umbria Marche region: Limits and capabilities
585 to unravel the subsurface structure in a seismically active area. *Annals of Geophysics*, 51(2–3), 383–396.
586 <https://doi.org/10.4401/ag-3032>, 2008.

587 Naeini E. Z. and Prindle, K.: Machine learning and learning from machines, *The Leading Edge*, 37:12, 886-893, 2018.

588 Patacca, E., and Scandone, P.: Late thrust propagation and sedimentary response in the thrust-belt foredeep system of the
589 southern Apennines (Pliocene–Pleistocene). In G. Vai & I. Martini (Eds.), *Anatomy of an Orogen: The Apennines and adjacent*
590 *Mediterranean basins*, 441–454, Norwell, MA: Kluwer Acad., 2001.

591 Pauselli, C., Barchi, M. R., Federico, C., Magnani, M. B. and Minelli, G.: The crustal structure of the northern Apennines
592 (Central Italy): An insight by the CROP03 seismic line. *American Journal of Science*, 306(6), 428–450.
593 <https://doi.org/10.2475/06.2006.02>, 2006.

594 Pauselli, C., Federico, C., Frigeri, A., Orosei, R., Barchi, M.R. & Basile, G.: Ground Penetrating Radar investigations to study
595 active faults in the Norcia Basin (Central Italy), *Journal of Applied Geophysics*, 72, 39-45, 2010.

596 Pierantoni, P. P., Deiana, G., & Galdenzi, S.: Stratigraphic and structural features of the Sibillini Mountains (Umbria–Marche
597 Apennines, Italy). *Italian Journal of Geosciences*, 132, 497–520. <https://doi.org/10.3301/IJG.2013.08>, 2013.

598 Pizzi, A., Calamita, F., Coltorti, M., & Pieruccini, P.: Quaternary normal faults, intramontane basins and seismicity in the
599 Umbria-MarcheAbruzzi Apennine Ridge (Italy): Contribution of neotectonic analysis to seismic hazard assessment. *Bollettino*
600 *Società Geologica Italiana Special Publication*, 1(January), 923–929, 2002.

601 Porreca, M., Minelli, G., Ercoli, M., Brobia, A., Mancinelli, P., Cruciani, F., Giorgetti, C., Carboni, C., Mirabella, F., Cavinato,
602 G., Cannata, A., Pauselli, C., Barchi, M.R.: Seismic reflection profiles and subsurface geology of the area interested by the
603 2016–2017 earthquake sequence (Central Italy). *Tectonics*, 37, 1-22, doi: 10.1002/2017TC004915, 2018.

604 Press, F., and D. Jackson: Alaskan earthquake, 27 March 1964: Vertical extent of faulting and elastic strain energy release,
605 *Science*, 147, 867, 1965.

606 Pucci, S, De Martini, P.M., Civico, R., Villani, F, Nappi, R., Ricci, T., Azzaro, R., Brunori, C. A., Caciagli, M., Cinti, F. R.,
607 Sapia, V., De Ritis, R., Mazzarini, F., Tarquini, S., Gaudiosi, G., Nave, R., Alessio, G., Smedile, A., Alfonsi, L., Cucci, L.,
608 Pantosti, D.: Coseismic ruptures of the 24 August 2016, Mw6.0 Amatrice earthquake (central Italy). *Geophysical Research*
609 *Letters*, American Geophysical Union (AGU), 2017.

610 Ramsay, J. G., Huber, M. I.: *The Techniques of Modern Structural Geology: Folds and Fractures*. Elsevier Science, 391 pp.,
611 1987.

612 Roure, F., P. Choukroune, X. Berastegui, J. A. Munoz, A. Villien, P. Matheron, M. Bareyt, M. Seguret, P. Camara, and J.
613 Deramond: Ecore deep seismic data and balanced cross sections: Geometric constraints on the evolution of the Pyrenees,
614 *Tectonics*, 8(1), 41–50, doi:10.1029/TC008i001p00041, 1989.

615 Rovida, A., Locati, M., Camassi, R., Lolli, B., & Gasperini P. (Eds.): CPTI15, the 2015 version of the parametric catalogue of
616 Italian earthquakes, Istituto Nazionale di Geofisica e Vulcanologia. <https://doi.org/10.6092/INGV.IT-CPTI15>, 2016.

617 Schwartz, D. P., & Coppersmith, K. J.: Fault behavior and characteristic earthquakes: Examples from the Wasatch and San
618 Andreas fault zones. *Journal of Geophysical Research: Solid Earth*, 89(B7), 5681-5698, 1984.

619 Serva L., Blumetti A.M., Guerrieri L. and Michetti A.M.: The Apennine intermountain basins: the result of repeated strong
620 earthquakes over a geological time interval. *Boll. Soc. Geol. It.*, 1, 939-946, 2002.

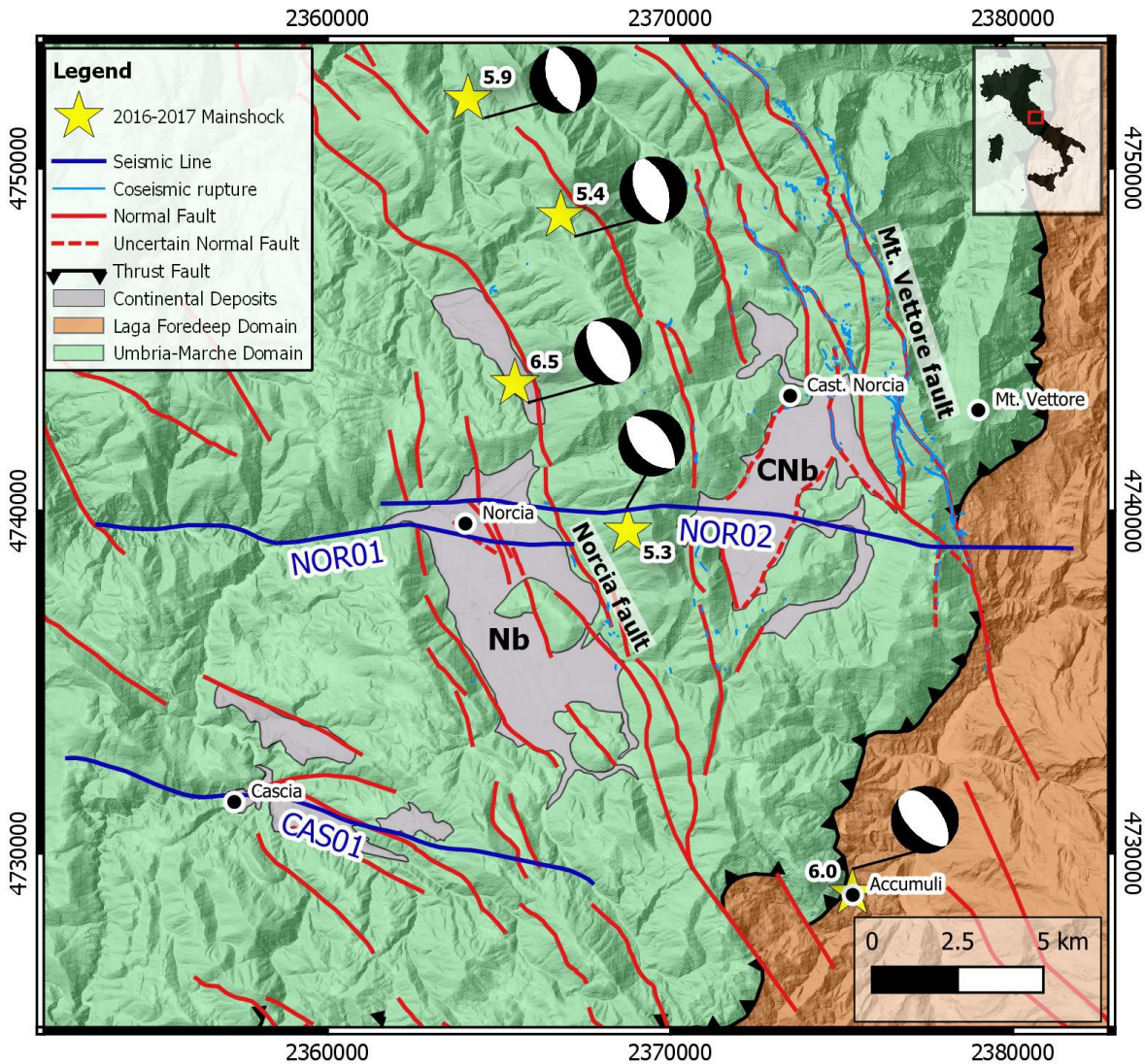
621 Simancas, J. F., Carbonell .R., González Lodeiro, F., Pérez Estaún, A., Juhlin, C., Ayarza, P., Kashubin, A., Azor, A., Martínez
622 Poyatos, D., Almodóvar, G.R., Pascual, E., Sáez, R., Expósito, I.: Crustal structure of the transpressional Variscan orogen of
623 SW Iberia: SW Iberia deep seismic reflection profile (IBERSEIS), *Tectonics*, 22, 1062, doi:10.1029/2002TC001479, 6, 2003.
624 Taner, M.T., Koehler, F., and Sheriff, R.E.: Complex Seismic Trace Analysis. *Geophysics*, 44 (6): 1041.
625 <http://dx.doi.org/10.1190/1.1440994>, 1979.
626 Taner, M.T.: Seismic attributes. *Canadian Society of Exploration Geophysicists Recorder*, 26. 48-56, 2001.
627 Tarquini, S., Isola, I., Favalli, M., & Boschi, E.: TINITALY/01: a new triangular irregular network of Italy. *Annals of*
628 *Geophysics*, 50–53, 2007.
629 Tarquini, S., Vinci, S., Favalli, M., Doumaz, F., Fornaciai, A., & Nannipieri, L.: Release of a 10-m-resolution DEM for the
630 Italian territory: Comparison with global-coverage DEMs and anaglyph-mode exploration via the web. *Computers and*
631 *Geosciences*, 38(1), 168–170. <https://doi.org/10.1016/j.cageo.2011.04.018>, 2012.
632 Trippetta, F., Collettini, C., Vinciguerra, S., & Meredith, P. G.: Laboratory measurements of the physical properties of Triassic
633 evaporites from Central Italy and correlation with geophysical data. *Tectonophysics*, 492(1), 121–132, 2010.
634 Torvela T., Moreau, J., Butler, R., W. H, Korja, A. and Heikkinen, P.: The mode of deformation in the orogenic mid-crust
635 revealed by seismic attribute analysis, *Geochem., Geophys., Geosyst.*, 14, 1069–1086, 2013.
636 Vai, G. B.: Basement and early (pre-Alpine) history. In G. B. Vai & I. P. Martini (Eds.), *Anatomy of an orogen: The Apennines*
637 *and adjacent Mediterranean basins*, 121–150, Dordrecht, Netherlands: Kluwer Academic Publisher.
638 https://doi.org/10.1007/978-94-015-9829-3_10, 2001.
639 Valoroso, L. et al. Radiography of a normal fault system by 64,000 high-precision earthquake locations: The 2009 L’Aquila
640 (central Italy) case study. *J. Geophys. Res. - Solid Earth*, 118, 1156–1176, <https://doi.org/10.1002/jgrb.50130>, 2013.
641 Vernengo, L., Trinchero, E., Torrejón, M. G., and Rovira, I.: Amplitude volume technique attributes and multidimensional
642 seismic interpretation. *The Leading Edge*, 36(9), 776–781. <https://doi.org/10.1190/tle36090776.1>, 2017.
643 Villani, F., Pucci, S., Civico, R., De Martini, P. M., Cinti, F. R., & Pantosti, D.: Surface faulting of the 30 October 2016 Mw
644 6.5 central Italy earthquake: Detailed analysis of a complex coseismic rupture. *Tectonics*, 37, 3378–3410.
645 <https://doi.org/10.1029/2018TC005175>, 2018a.
646 Villani, F., Sapia, V., Baccheschi, P., Civico, R., Di Giulio, G., Vassallo, M., et al.: Geometry and structure of a fault bounded
647 extensional basin by integrating geophysical surveys and seismic anisotropy across the 30 October 2016 Mw 6.5 earthquake
648 fault (central Italy): The Pian Grande di Castelluccio basin. *Tectonics*, 37. <https://doi.org/10.1029/2018TC005205>, 2018b.
649 Yi, S., Wu, C., Li, Y. et al. *J. Mt. Sci.*: Source tectonic dynamics features of Jiuzhaigou Ms 7.0 earthquake in Sichuan Province,
650 China, *Journal of Mountain Science*, 15(10): 2266-2275. doi: 10.1007/s11629-017-4703-6, 2018.
651 Wilkinson, M. W., McCaffrey, K. J. W., Jones, R. R., Roberts, G. P., Holdsworth, R. E., Gregory, L. C., et al.: Near-field fault
652 slip of the 2016 Vettore Mw 6.6 earthquake (Central Italy) measured using low-cost GNSS. *Scientific Reports*, 7(1), 4612,
653 doi:10.1038/s41598-017-04917-w, 2017.

654 Wrona, T., Pan, I., Gawthorpe, R. L. and Fossen, H.: Seismic facies analysis using machine learning, *Geophysics*, 83:5, O83-
 655 O95, 2018.

656 Wyss, M. and Brune, J. N.: The Alaska earthquake of 28 March 1964: A complex multiple rupture, *Bull. Seism. Soc. Amer.*
 657 57, (5), 1967.

658 Zhao, W., Forte, E., Fontolan, G., Pipan, M.: Advanced GPR imaging of sedimentary features: integrated attribute analysis
 659 applied to sand dunes, *Geophysical Journal International*, 213:1, 147–156, <https://doi.org/10.1093/gji/ggx541>, 2018.

660 ---



661 **Figure 1**

662
 663

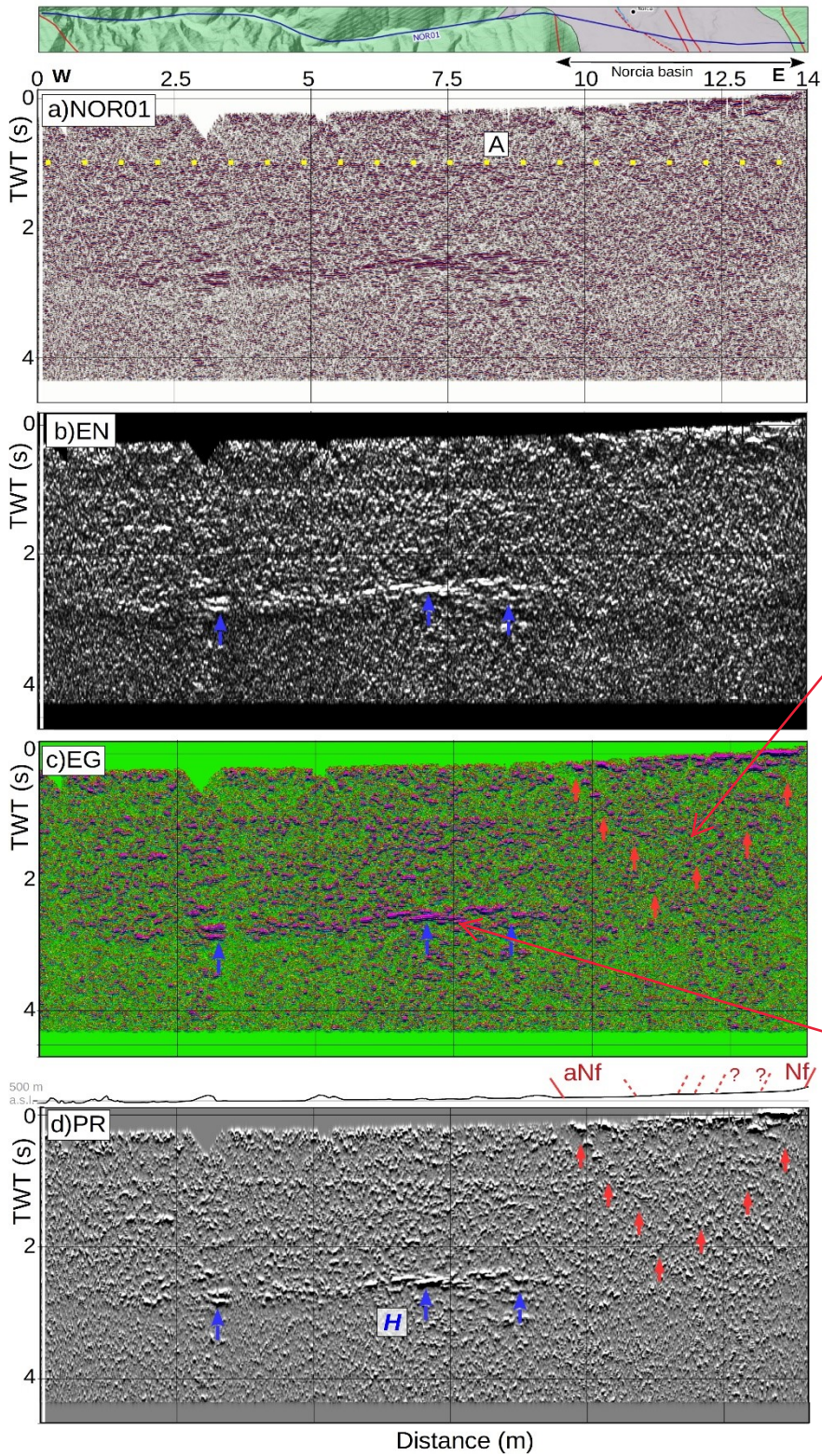


Figure 2

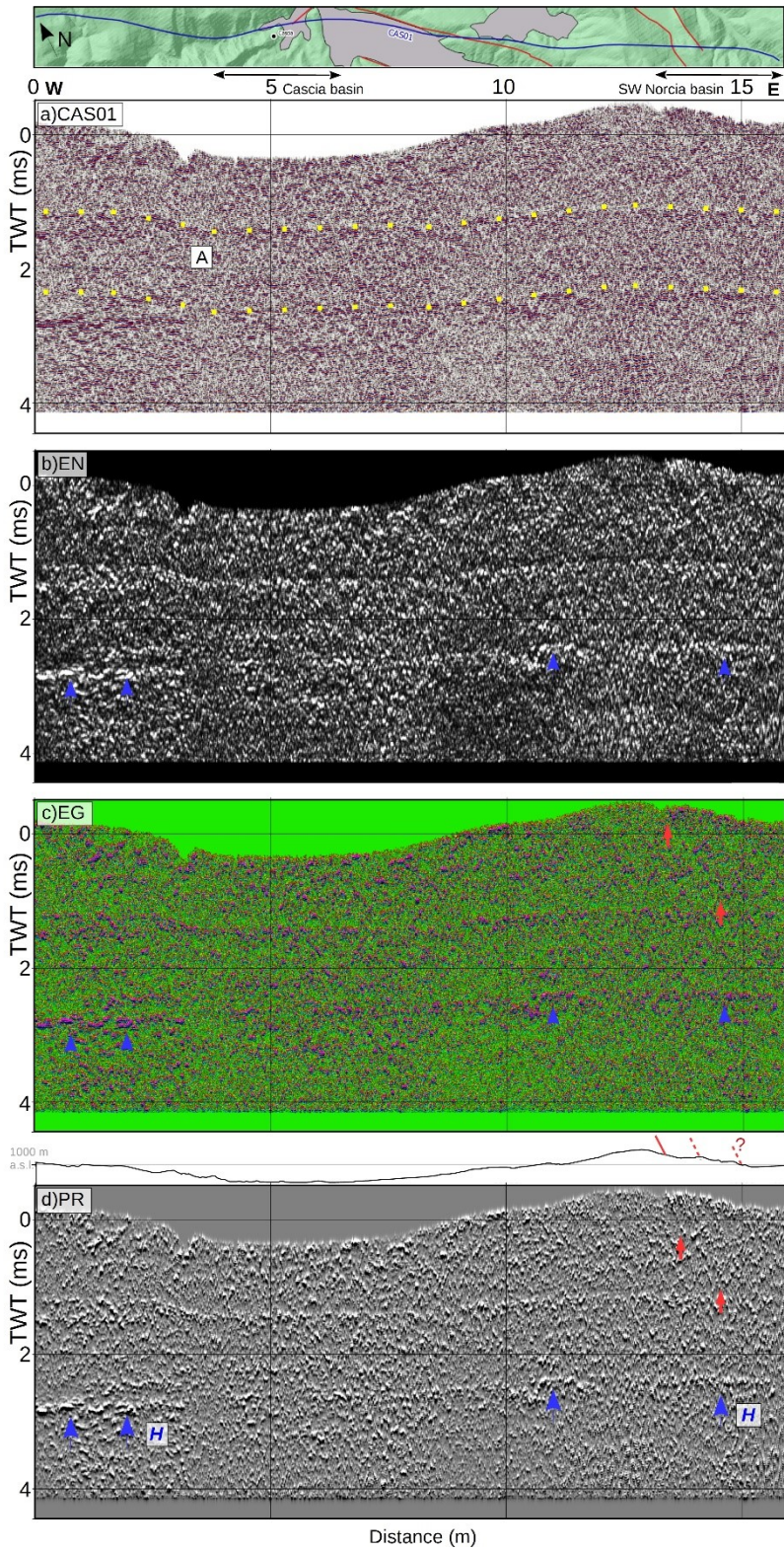


Figure 3

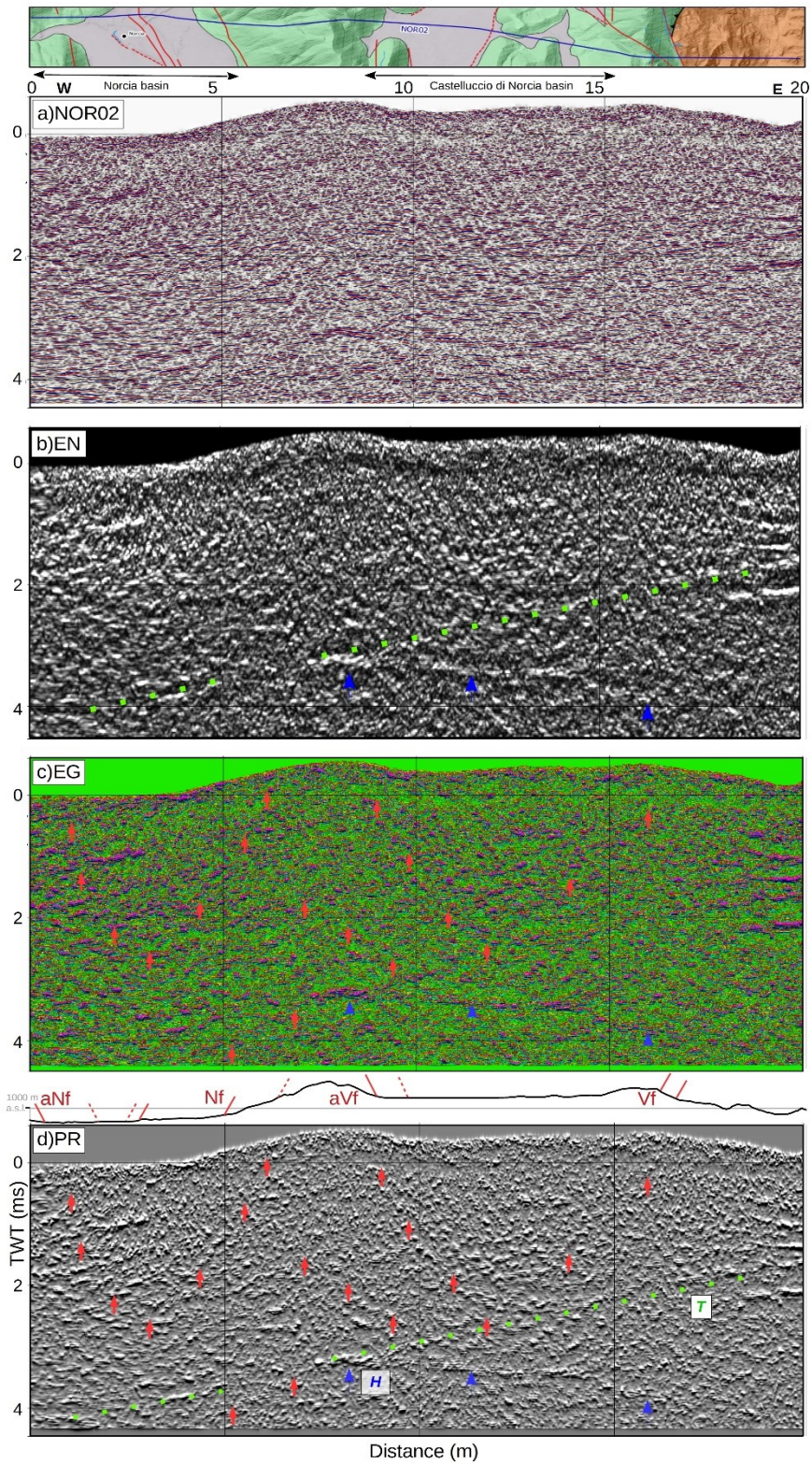
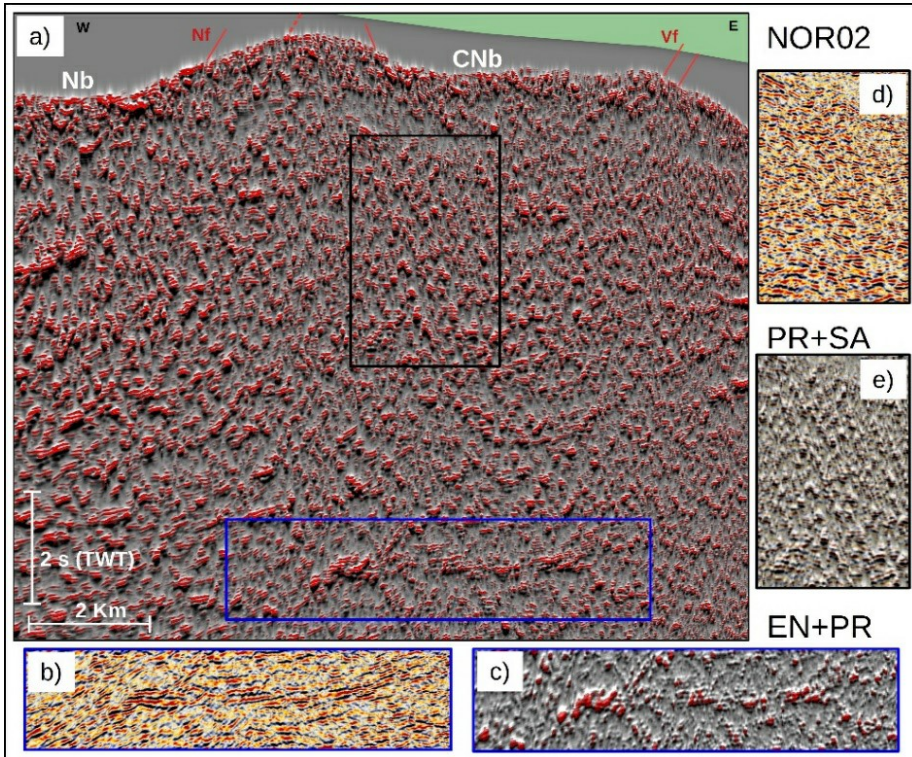


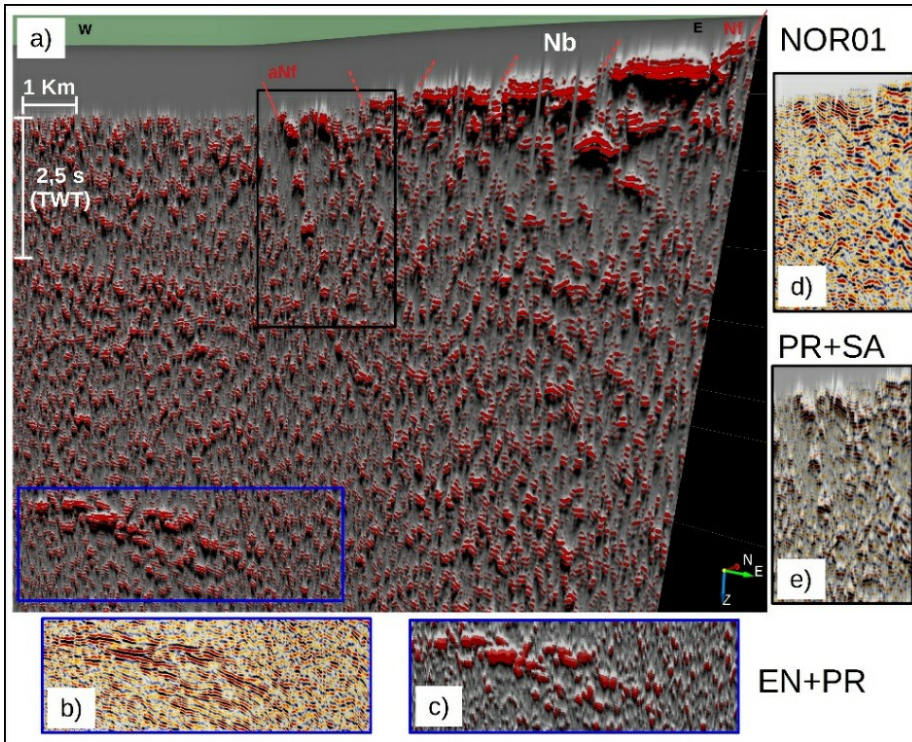
Figure 4

667



668

Figure 5

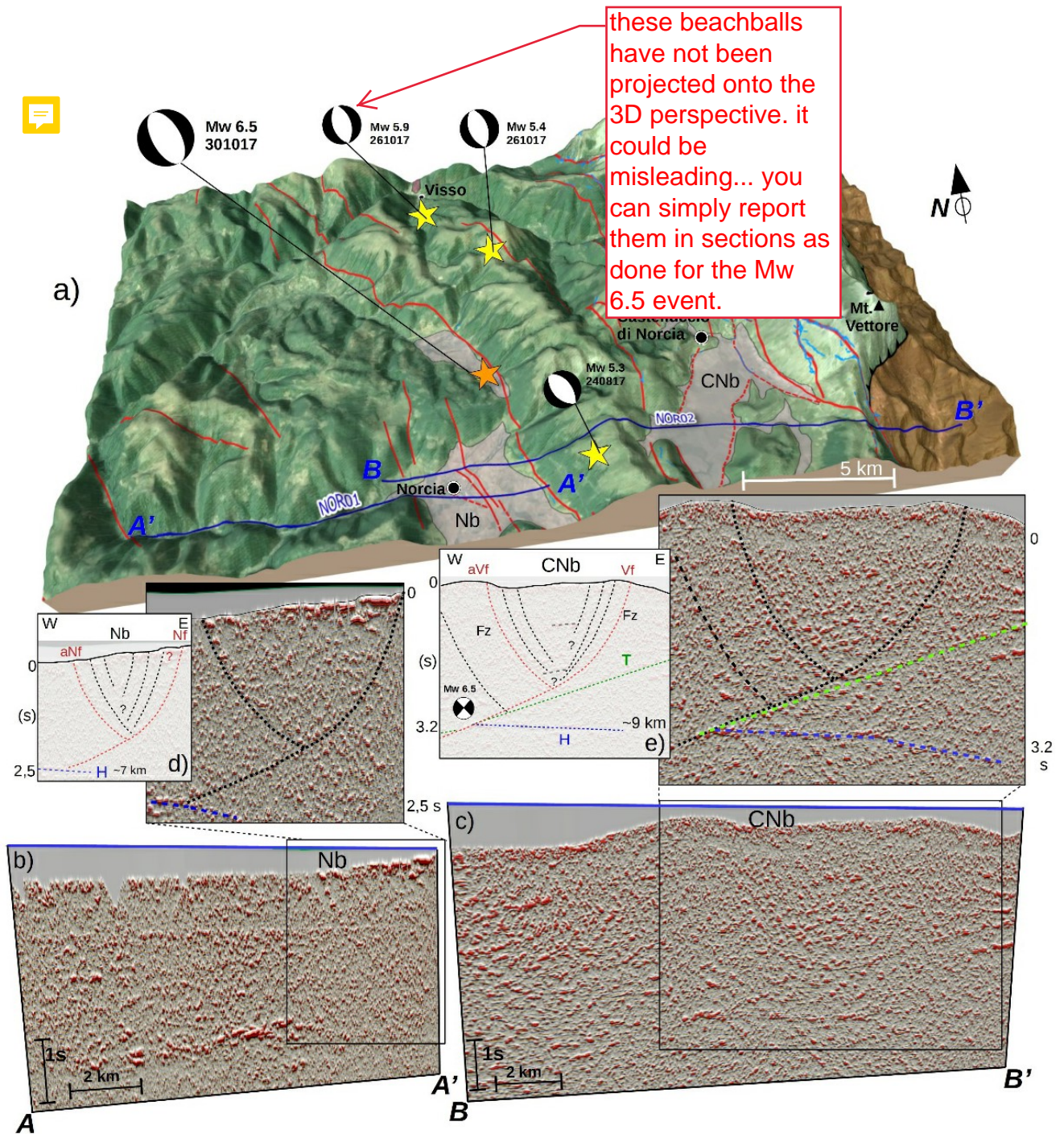


669

Figure 6

670

671

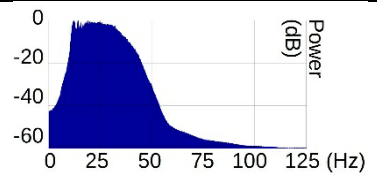
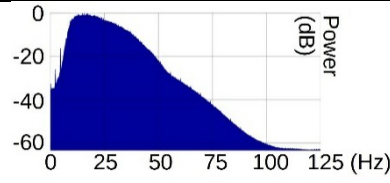
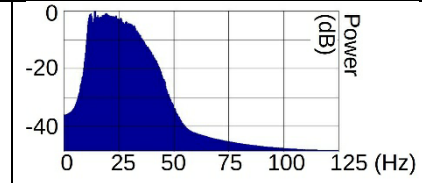


672

673

674

Figure 7

| Parameters | NOR01 | NOR02 | CAS01 |
|------------------------------|---|--|---|
| Source | Vibroseis | Vibroseis | Explosive |
| Length (km) | 14 | 20 | 16 |
| Number of traces | 938 | 825 | 1069 |
| Samples/trace | 1600 | 1750 | 1600 |
| Time window (ms) | 6400 | 7000 | 6400 |
| Sampling interval (ms) | 4 | 4 | 4 |
| Trace interval (m) | 15 | 25 | 15 |
| Mean Spectral amplitude (dB) |  |  |  |

676

677 **Figures and Tables captions:**

678 **Figure 1: Simplified geological map of the study area (modified after Porreca et al., 2018), showing the 2D seismic data tracks, the**
679 **2016-2017 mainshock locations, beachballs, and magnitudes, the surface ruptures and the known master faults. Nb Norcia basin,**
680 **CNb Castelluccio di Norcia basin.**

681 **Figure 2: Stack version of NOR01; a) reflection amplitude, yellow dots underline a processing artefact (A); b) Energy attribute**
682 **enhancing a strong reflectivity contrasts (H, blue arrows); c) Energy Gradient, improving the detection of dipping alignments and**
683 **continuity of reflectors; d) Pseudo-Relief enhancing the reflection patterns cross-cut by steep discontinuities (red arrows). Nf Norcia**
684 **fault, aNf antithetic Norcia fault.**

685 **Figure 3: Stack version of CAS01, with same attributes computation: a) reflection amplitude (yellow dots display processing**
686 **artefacts); b) Energy attribute c) Energy Gradient attribute; d) Pseudo-Relief, showing the strong regional reflector H (blue arrows).**
687 **A high-angle discontinuity on the western margin is interpretable as a normal fault, showing an attribute signature analogous to**
688 **aNf.**

689 **Figure 4: Time migrated version of NOR02; a) reflection amplitude; b) Energy attribute displaying the reflector H (blue arrows)**
690 **and a possible low angle discontinuity (T, green dots); c) Energy Gradient attribute, showing the master faults bounding the basins**
691 **(red arrows); d) Pseudo-Relief, improving the reflectors continuity/discontinuity and the master faults display (red arrows). Nf**
692 **Norcia fault, aNf antithetic Norcia fault; Vf Mt. Vettore fault, aVf antithetic Mt. Vettore fault.**

693 **Figure 5: Multi-attribute display of NOR02; a) EN+PR attributes, the seismic facie in the blue box is compared with the original**
694 **seismic line (b) and EN+PR (c) for comparison; the same plot for the black box is reported in figures d) and e) (original line and**
695 **PR+SA, respectively).**

696 **Figure 6: Multi-attribute display of NOR01; a) EN+PR attributes, the seismic facie in the blue box showing a strong set of deep**
697 **reflectors is compared with the original seismic line in b) and EN+PR c). An analogous plot of the black box reports in figures d)**
698 **and e) the original line and the combination PR+SA.**

699 **Figure 7: Integration of surface and subsurface data (DTM by Tarquini et al., 2012); a) 3D-view of a W-E section crossing Nb and**
700 **CNb, and the mainshock locations (ISIDE working group, 2016). Surface and deep data allow to correlate the master faults and**
701 **coseismic ruptures at the surface. The multi-attribute display of NOR01 (b) and NOR02 (c), is obtained overlapping the reflection**
702 **amplitude in transparency with the Pseudo-Relief and Energy attributes (red palette). A significative improvement of the subsurface**
703 **images provides unprecedented details on the seismogenic fault zones: the two conjugate basins show master faults along the borders**
704 **and some minor synthetic and antithetic splays (see d) and e) sketches).**

705 **Table 1: List of some parameters extracted from SEG-Y headers and three mean frequency spectra of the three seismic lines. An**
706 **approximate vertical resolution equal to 80 m was derived ($v=6$ km/s).**